A FINITE ELEMENT MODEL FOR INVERSE DESIGN PROBLEMS IN LARGE DEFORMATIONS ANISOTROPIC HYPERELASTICITY

Víctor D. Fachinotti[a], Alberto Cardona[a] and Philippe Jetteur[b]

[a]*Centro Internacional de Métodos Computacionales en Ingeniería (CIMEC-INTEC), Universidad Nacional del Litoral - CONICET, Güemes 3450, CP 3000, Santa Fe, Argentina*
[b]*Samtech SA, Parc Scientifique du Sart Tilman, Rue des Chasseurs-Ardennals, 8, B 4031, Angleur, Liège, Belgium*

Keywords: Inverse design, anisotropic, hyperelastic, large deformation, finite element method.

Abstract. This paper introduces a finite element model for the inverse design of pieces with large displacements in the elastic range. The problem consists in determining the initial shape of the piece, such that it attains the designed shape under the effect of service loads. The model is particularly focused on the design of pieces with a markedly anisotropic behavior, like laminated turbine blades. The formulation expresses equilibrium on the distorted configuration. However, it uses the standard constitutive equation library, which is usually expressed for measures attached to the undistorted configuration. Modifications in standard finite elements codes are then restricted to the routines for the computation of the finite element internal forces and tangent matrix. Two application examples are given, the first one for validation purposes, while the second application has industrial interest for the design of turbine blades.

1 INTRODUCTION

A central aspect when we design a piece to have a certain shape after severe deformation, is to know the undistorted shape of this piece. In this analysis, the final (desired) configuration is supposed to be that of the piece subjected to service loads once the steady state has been attained, neglecting any transient effect.

The classical (direct) problem in nonlinear elasticity consists in determining the distorted shape knowing the loads applied to the piece in a given reference configuration. The subject of this study is the inverse problem that consists in determining the undistorted configuration knowing the final configuration and service loads. Strictly speaking, it is an inverse "design" problem (Beck and Woodbury, 1998), in contrast to classical inverse "measurement" problems (often called simply "inverse problems"), consisting in determining the material data knowing both the distorted and undistorted configurations, as well as the service loads.

Some pieces (like turbine blades) that are designed to be cyclically used, must recover the original shape after each service cycle. This constraints the material of these pieces to lie into the elastic range all along the deformation process. Moreover, sometimes they are made of laminates, with a markedly orthotropic behavior. Therefore, with the restriction of being limited to small strains but large deformations, we will use an anisotropic hyperelastic material law. We remark that in the isotropic case, some simplifications could be introduced that allow extending the formulation to finite hyperelasticity.

Previous numerical models for the inverse design analysis of hyperelastic bodies subjected to large deformations have been proposed by Govindjee and Mihalic (1996, 1998) and Yamada (1997). Both models use the finite element method in order to discretize the inverse deformation. They differ in the fact that Govindjee and Mihalic's model is Eulerian, because the equilibrium equation is formulated in terms of variables attached to the (known) distorted configuration, while Yamada's model is Arbitrary-Lagrangean-Eulerian (ALE), i.e., the problem is expressed on a reference configuration which is different from the undistorted and distorted ones.

The additional complexity involved by the third configuration inherent to the ALE model, makes the Eulerian model better suited for current applications. Indeed, we began by following Govindjee and Mihalic (1998) until some practical constraints in the modelling of anisotropic media motivated the current development. First, Govindjee and Mihalic (1998) write not only the equilibrium equations but also the constitutive equations in terms of Eulerian variables, which complicates the description of orthotropic materials whose preferred directions are usually defined in the unknown undistorted configuration. As it will be shown in Section 3.1, this gives rise to an additional source of nonlinearity that has not been considered up-to-date.

An effort has been made in order to use the available material library from our nonlinear finite elements code Mecano (Samtech, 2005), in which constitutive equations are written in terms of Lagrangean variables. Then, the modifications made into the code in order to implement the current model are restricted to the routines for computing the residual vector and tangent matrix for the inverse finite element method, preserving the material library.

The other important contribution is the treatment of body forces, not included in the previous works. In fact, in the problems addressed by the previous inverse design models (Govindjee and Mihalic, 1996, 1998; Yamada, 1997), the body forces were not relevant. However, this is not the case when modelling turbine blades, where centrifugal body forces are significant. External forces (including body and surface forces) usually depend on deformation, with the consequent contribution to the finite element tangent matrix.
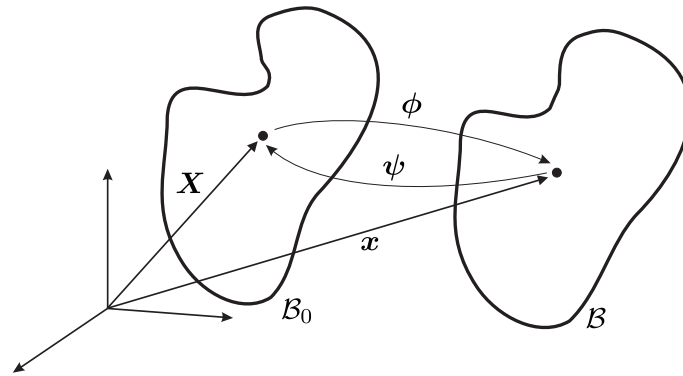
Figure 1: Distorted configuration $\mathcal{B}$, domain of inverse analysis, and undistorted configuration $\mathcal{B}_0$ sought as solution.

Two examples of application of the model are given. First, we consider the simple case of bending of a laminated beam, for which the determination of its distorted shape is an easy task for any available code for large deformation analysis. Once the distorted shape is known, we evaluate the ability of the present model to recover the initial shape. The second case is an industrial application to the determination of the initial shape that a laminated turbine blade should have in order to attain the desired designed shape under pressure and centrifugal loads.

2 KINEMATIC DESCRIPTION

Let $\mathcal{B}_0$ be the undistorted reference configuration of a continuum body, and $\mathcal{B}$ the objective (final) configuration. The position $\boldsymbol{x} \in \mathcal{B}$ of any particle P with position $\boldsymbol{X} \in \mathcal{B}_0$ is determined by the deformation $\boldsymbol{x} = \boldsymbol{\phi}(\boldsymbol{X})$. The deformation gradient relative to the reference configuration is :

$$\boldsymbol{F} = \operatorname{Grad} \boldsymbol{\phi}, \tag{1}$$

where Grad denotes gradient with respect to $\boldsymbol{X} \in \mathcal{B}_0$.

In the problem we are interested in, we know the final configuration and we want to determine the inverse deformation $\boldsymbol{X} = \boldsymbol{\psi}(\boldsymbol{x})$ giving the position $\boldsymbol{X} \in \mathcal{B}_0$ of every particle whose final position is $\boldsymbol{x} \in \mathcal{B}$. The inverse deformation gradient is defined as

$$\boldsymbol{f} = \operatorname{grad} \boldsymbol{\psi} = \boldsymbol{F}^{-1}, \tag{2}$$

where grad denotes gradient with respect to $\boldsymbol{x} \in \mathcal{B}$.

3 MATERIAL DESCRIPTION

The constitutive law for a general hyperelastic material can be written as follows (Ogden, 1997)

$$\boldsymbol{S} = \frac{\partial w}{\partial \boldsymbol{E}} = \boldsymbol{S}(\boldsymbol{E}), \tag{3}$$

where w is the strain-energy density function, $\boldsymbol{S}$ is the second Piola-Kirchhoff stress tensor, and $\boldsymbol{E}$ is the Green-Lagrange strain tensor defined as

$$\boldsymbol{E} = \frac{1}{2} \left(\boldsymbol{F}^T \boldsymbol{F} - \boldsymbol{1} \right), \tag{4}$$

$\boldsymbol{1}$ denoting the second-order identity tensor.

3.1 Accounting for anisotropy in inverse modelling

The constitutive equation (3) is formulated in terms of S and E, that are Lagrangean tensors, i.e. tensors related to the reference configuration. Consequently, the material properties must be attached to this configuration which is unknown. This hinders the definition of preferred material directions, and hence the modelling of anisotropic materials.

Fortunately, in the case of laminated bodies like turbine blades, although we may have very large rotations, strains remain small. Then, it is possible to estimate accurately the preferred directions in the distorted configuration by writing the constitutive equation (3) in Eulerian form by simple rotation of the material axes. Therefore, we rotate the Green-Lagrange strain tensor and the second Piola-Kirchhoff stress tensor to the spatial axes as follows :

$$E^* = RER^T = \frac{1}{2}\left(FF^T - 1\right) = \frac{1}{2}\left(V^2 - 1\right), \tag{5}$$

$$S^* = RSR^T. \tag{6}$$

V is the symmetric positive-definite left-stretch tensor, and R is the proper orthogonal rotation tensor, both arising from the polar decomposition of the deformation gradient :

$$F = VR. \tag{7}$$

Now, the chain rule together with equation (5) yields

$$S_{ij} = \frac{\partial w}{\partial E_{ij}} = \frac{\partial w}{\partial E_{kl}^*}\frac{\partial E_{kl}^*}{\partial E_{ij}} = R_{ki}R_{lj}\frac{\partial w}{\partial E_{kl}^*}, \quad \text{or} \quad S = R^T\frac{\partial w}{\partial E^*}R, \tag{8}$$

from which we deduce the desired constitutive law in Eulerian form :

$$S^* = \frac{\partial w}{\partial E^*} = S^*(E^*). \tag{9}$$

In such a way, we are able to define the material properties with respect to a system of axes linked to the known distorted configuration.

4 FINITE ELEMENT FORMULATION

The inverse design problem consists in finding the function ψ that satisfies the equilibrium equations, taken here in the weak form :

$$\int_{\mathcal{B}} \text{tr}\left[\sigma^T\text{grad}(\eta)\right]dv - \int_{\mathcal{B}} b\cdot\eta\,dv - \int_{\partial\mathcal{B}_t} t\cdot\eta\,ds = 0 \tag{10}$$

for every admissible variation η, where σ is the Cauchy stress tensor, b is the given body force per unit distorted volume, t is the traction prescribed on the portion $\partial\mathcal{B}_t$ of the boundary $\partial\mathcal{B}$ of the distorted domain $\mathcal{B}$ (hence, t is a force per unit distorted area).

Using the finite element method, the position of particles in the undistorted configuration is approximated inside a typical finite element Ω^e with nodes $1, 2, \ldots, N$ as follows

$$X \approx \sum_{I=1}^N N_I(x)X_I, \tag{11}$$

where $N_I(x)$ is the shape function associated to the node I, and X_I is the unknown position of this node in the undistorted configuration.

Introducing this approximation, and taking variations with respect to the positions in the undistorted configuration (that is, the standard Galerkin formulation), we get the discrete equation

$$\boldsymbol{R} = \boldsymbol{F}^{\text{int}} - \boldsymbol{F}^{\text{ext}} = \boldsymbol{0}, \tag{12}$$

where $\boldsymbol{F}^{\text{int}}$ and $\boldsymbol{F}^{\text{ext}}$ are respectively the internal and external force vectors, given by

$$\boldsymbol{F}^{\text{int}} = \int_{\mathcal{B}} \boldsymbol{B}^T \bar{\boldsymbol{\sigma}} \, \mathrm{d}v, \tag{13}$$

$$\boldsymbol{F}^{\text{ext}} = \int_{\mathcal{B}} \boldsymbol{N}^T \boldsymbol{b} \, \mathrm{d}v + \int_{\partial \mathcal{B}_t} \boldsymbol{N}^T \boldsymbol{t} \, \mathrm{d}s, \tag{14}$$

$\boldsymbol{B}$ being the well-known gradient matrix, and $\bar{\boldsymbol{\sigma}}$ the vector containing the independent components of the symmetric Cauchy stress tensor $\boldsymbol{\sigma}$, given as follows [1]

$$\bar{\boldsymbol{\sigma}} = [\sigma_{11} \ \sigma_{22} \ \sigma_{33} \ \sigma_{12} \ \sigma_{23} \ \sigma_{31}]^T.$$

The computation of $\boldsymbol{\sigma}$ is detailed in the next section.

Concerning external forces in turbine blades modelling, they mainly consist of the centrifugal and pressure forces. The former are represented by the first term of the r.h.s. of equation (14) with $\boldsymbol{b}$ defined as

$$\boldsymbol{b} = \rho \boldsymbol{a}^{\text{centr}}, \tag{15}$$

being ρ the density in the distorted configuration, and $\boldsymbol{a}^{\text{centr}}$ the centrifugal acceleration, defined as

$$\boldsymbol{a}^{\text{centr}}(\boldsymbol{x}) = \boldsymbol{\omega} \times [\boldsymbol{\omega} \times (\boldsymbol{x} - \boldsymbol{o})], \tag{16}$$

where $\boldsymbol{\omega}$ is the angular velocity vector and $\boldsymbol{o}$ the position of an arbitrary point on the rotation axis.

On the other hand, the second term of the r.h.s. of equation (14) represents the pressure force by defining

$$\boldsymbol{t} = -p\boldsymbol{n} \tag{17}$$

where p is the pressure and $\boldsymbol{n}$ the outer normal to the portion $\partial \mathcal{B}_t$ of the surface of the body in the distorted configuration.

4.1 Computation of strains and stresses in finite elements

By using equation (11), the inverse deformation gradient is approximated in terms of derivatives of the interpolation functions as :

$$\boldsymbol{f} = \frac{\partial \boldsymbol{X}}{\partial \boldsymbol{x}} \approx \frac{\partial N_I}{\partial \boldsymbol{x}} \boldsymbol{X}_I. \tag{18}$$

---

[1]From now on, in order to perform the matrix operations involved in the finite element formulation, every symmetric stress tensor will be mapped into a vector in the same way as $\boldsymbol{\sigma}$. Further, the strain tensor $\boldsymbol{E}$ (and any other symmetric strain tensor) will be mapped into the vector

$$\bar{\boldsymbol{E}} = [E_{11} \ E_{22} \ E_{33} \ 2E_{12} \ 2E_{23} \ 2E_{31}]^T.$$

Once $\boldsymbol{f}$ is known, we can compute the (direct) deformation gradient $\boldsymbol{F} = \boldsymbol{f}^{-1}$, and then the Green-Lagrange strain $\boldsymbol{E}$ using equation (4) as well as its rotated counterpart $\boldsymbol{E}^*$ given by equation (5).

Entering $\boldsymbol{E}^*$ in the constitutive law (9), we determine the rotated second Piola-Kirchhoff stress $\boldsymbol{S}^*$. Then, we are able to compute the Cauchy stress by means of the relationship

$$\boldsymbol{\sigma} = j\boldsymbol{F}\boldsymbol{S}\boldsymbol{F}^T = j\boldsymbol{V}\boldsymbol{S}^*\boldsymbol{V}^T, \tag{19}$$

or, given in Cartesian components :

$$\sigma_{kl} = jV_{km}S^*_{mn}V_{ln} = jI^V_{klmn}S^*_{mn}, \tag{20}$$

where $j = \det \boldsymbol{f}$ is the Jacobian of the inverse deformation $\boldsymbol{X} = \boldsymbol{\psi}(\boldsymbol{x})$, and

$$I^V_{klmn} = \frac{1}{2}\left(V_{km}V_{ln} + V_{kn}V_{lm}\right) = I^V_{klnm} = I^V_{lkmn}, \tag{21}$$

are the components of the fourth-order tensor $\boldsymbol{I}^V$, which verifies the stated relations of symmetry.

From equation (20), the following algorithmic matrix expression for the Cauchy stress is derived :

$$\bar{\boldsymbol{\sigma}} = j\bar{\boldsymbol{I}}^V\bar{\boldsymbol{S}}^*, \tag{22}$$

where $\bar{\boldsymbol{S}}^*$ is the vector of independent components of the symmetric stress tensor $\boldsymbol{S}^*$, and $\bar{\boldsymbol{I}}^V$ takes the form

$$\bar{\boldsymbol{I}}^V = \begin{bmatrix} I^V_{1111} & I^V_{1122} & I^V_{1133} & 2I^V_{1112} & 2I^V_{1123} & 2I^V_{1131} \\ I^V_{2211} & I^V_{2222} & I^V_{2233} & 2I^V_{2212} & 2I^V_{2223} & 2I^V_{2231} \\ I^V_{3311} & I^V_{3322} & I^V_{3333} & 2I^V_{3312} & 2I^V_{3323} & 2I^V_{3331} \\ I^V_{1211} & I^V_{1222} & I^V_{1233} & 2I^V_{1212} & 2I^V_{1223} & 2I^V_{1231} \\ I^V_{2311} & I^V_{2322} & I^V_{2333} & 2I^V_{2312} & 2I^V_{2323} & 2I^V_{2331} \\ I^V_{3111} & I^V_{3122} & I^V_{3133} & 2I^V_{3112} & 2I^V_{3123} & 2I^V_{3131} \end{bmatrix}. \tag{23}$$

Finally, the internal forces vector for the inverse finite element model can be written as

$$\boldsymbol{F}^{\text{int}} = \int_{\mathcal{B}} j\boldsymbol{B}^T\bar{\boldsymbol{I}}^V\bar{\boldsymbol{S}}^* \, \mathrm{d}v. \tag{24}$$

4.2   Solution of the nonlinear equilibrium equation

The nonlinear equation (12) is solved iteratively using the Newton-Raphson method (see Zienkiewicz and Taylor (2000) for details on the implementation of this method in the finite element context). At each iteration k we have to solve the following linear equation for the increment $\Delta\boldsymbol{q}$:

$$\boldsymbol{R}(\boldsymbol{q}^{k+1}) = \boldsymbol{R}(\boldsymbol{q}^k) + \boldsymbol{K}(\boldsymbol{q}^k)\Delta\boldsymbol{q}, \tag{25}$$

where $\boldsymbol{K}$ denotes the tangent matrix, given by :

$$\boldsymbol{K} = \frac{\partial\boldsymbol{R}}{\partial\boldsymbol{q}} = \frac{\partial\boldsymbol{F}^{\text{int}}}{\partial\boldsymbol{q}} + \frac{\partial\boldsymbol{F}^{\text{ext}}}{\partial\boldsymbol{q}} = \boldsymbol{K}^{\text{int}} + \boldsymbol{K}^{\text{ext}}. \tag{26}$$

and where $\boldsymbol{q}$ is the vector of unknown nodal parameters, which in this case are the positions $\boldsymbol{X}_I$ of nodes at the initial configuration.

Concerning external forces, we note that there is no contribution to the tangent matrix from the pressure forces in inverse modelling. In fact, contrary to what happens in direct modelling, the normal $\boldsymbol{n}$ to the external surface in the distorted configuration is known and fixed. On the other hand, there would be no contribution from the centrifugal force vector if ρ were known in the distorted configuration. However, the value of the density we usually know is that related to the undistorted configuration, say ρ_0. Then, ρ is computed from the local mass balance equation

$$\rho = j\rho_0. \tag{27}$$

Nevertheless, if we remain within the domain of small strains, just a slight variation of the density is expected, so $\rho \approx \rho_0$ and the contribution of the centrifugal forces to the tangent matrix can be neglected.

Therefore, the tangent matrix reduces to the expression

$$\boldsymbol{K} \approx \boldsymbol{K}^{\text{int}} = \int_{\mathcal{B}} \boldsymbol{B}^T \frac{\partial \bar{\boldsymbol{\sigma}}}{\partial \boldsymbol{q}} \, \mathrm{d}v. \tag{28}$$

The computation of $\partial \bar{\boldsymbol{\sigma}}/\partial \boldsymbol{q}$ in an exact analytical way is described in the next section.

4.3 Computation of the stress derivatives

In a typical finite element, after computing the internal forces vector as described above, we know the inverse deformation gradient $\boldsymbol{f}$, the deformation gradient $\boldsymbol{F}$, the left-stretch tensor $\boldsymbol{V}$ and the fourth-order tensor $\boldsymbol{I}^V$ (which is a function of $\boldsymbol{V}$ squared), the rotated Green-Lagrange strain $\boldsymbol{E}^*$, the rotated Piola-Kirchhoff stress $\boldsymbol{S}^*$ and the Cauchy stress $\boldsymbol{\sigma}$. In order to compute the tangent stiffness matrix for inverse analysis, we need to compute the derivatives of the Cauchy stress, given in vector form by equation (22), with respect to the nodal parameters of the inverse motion. For this purpose, we will compute first the corresponding variations :

$$\Delta\boldsymbol{\sigma} = \Delta(jI^V_{klmn}S^*_{mn}) = \frac{1}{j}\boldsymbol{\sigma}\Delta j + j\boldsymbol{I}^V\Delta\boldsymbol{S}^* + j\Delta\boldsymbol{I}^V\boldsymbol{S}^*. \tag{29}$$

This can be written in the matrix form

$$\Delta\bar{\boldsymbol{\sigma}} = \bar{\boldsymbol{\Delta}}^{(1)} + \bar{\boldsymbol{\Delta}}^{(2)} + \bar{\boldsymbol{\Delta}}^{(3)}, \tag{30}$$

where $\bar{\boldsymbol{\Delta}}^{(i)}$ is the algorithmic counterpart of the i-th term of equation (29). For clarity, the computation of each term will be treated separately.

4.3.1 Computation of $\bar{\boldsymbol{\Delta}}^{(1)}$.

The differentiation rule for the determinant of a second order tensor yields

$$\Delta j = j \,\, \mathrm{tr}\,(\boldsymbol{F}^T\Delta\boldsymbol{f}) = j \,\, \bar{\boldsymbol{F}}^T\Delta\bar{\boldsymbol{f}}. \tag{31}$$

with

$$\bar{\boldsymbol{F}}^T = [F_{11} \,\, F_{12} \,\, F_{13} \,\, F_{21} \,\, F_{22} \,\, F_{23} \,\, F_{31} \,\, F_{32} \,\, F_{33}] \tag{32}$$

and

$$\Delta \bar{\boldsymbol{f}} = \begin{bmatrix} \Delta f_{11} \\ \Delta f_{21} \\ \Delta f_{31} \\ \Delta f_{12} \\ \Delta f_{22} \\ \Delta f_{32} \\ \Delta f_{13} \\ \Delta f_{23} \\ \Delta f_{33} \end{bmatrix}. \tag{33}$$

Further, after differentiating equation (18), we get

$$\Delta \boldsymbol{f} = \frac{\partial N_I}{\partial \boldsymbol{x}} \Delta \boldsymbol{X}_I, \tag{34}$$

which can be written in the matrix form

$$\Delta \bar{\boldsymbol{f}} = \begin{bmatrix} \frac{\partial N_1}{\partial x} & 0 & 0 & \frac{\partial N_2}{\partial x} & 0 & 0 & \cdots \\ 0 & \frac{\partial N_1}{\partial x} & 0 & 0 & \frac{\partial N_2}{\partial x} & 0 & \cdots \\ 0 & 0 & \frac{\partial N_1}{\partial x} & 0 & 0 & \frac{\partial N_2}{\partial x} & \cdots \\ \frac{\partial N_1}{\partial y} & 0 & 0 & \frac{\partial N_2}{\partial y} & 0 & 0 & \cdots \\ 0 & \frac{\partial N_1}{\partial y} & 0 & 0 & \frac{\partial N_2}{\partial y} & 0 & \cdots \\ 0 & 0 & \frac{\partial N_1}{\partial y} & 0 & 0 & \frac{\partial N_2}{\partial y} & \cdots \\ \frac{\partial N_1}{\partial z} & 0 & 0 & \frac{\partial N_2}{\partial z} & 0 & 0 & \cdots \\ 0 & \frac{\partial N_1}{\partial z} & 0 & 0 & \frac{\partial N_2}{\partial z} & 0 & \cdots \\ 0 & 0 & \frac{\partial N_1}{\partial z} & 0 & 0 & \frac{\partial N_2}{\partial z} & \cdots \end{bmatrix} \begin{bmatrix} \Delta X_{1x} \\ \Delta X_{1y} \\ \Delta X_{1z} \\ \Delta X_{2x} \\ \Delta X_{2y} \\ \Delta X_{2z} \\ \Delta X_{3x} \\ \Delta X_{3y} \\ \vdots \end{bmatrix} = \boldsymbol{N}_{,x} \Delta \boldsymbol{q}. \tag{35}$$

So, the variation of j takes the form

$$\Delta j = j \bar{\boldsymbol{F}}^T \Delta \bar{\boldsymbol{f}} = j \bar{\boldsymbol{F}}^T \boldsymbol{N}_{,x} \Delta \boldsymbol{q}, \tag{36}$$

Then, the first term in the r.h.s. of equation (29) can be expressed in the matrix form

$$\bar{\boldsymbol{\Delta}}^{(1)} = \frac{1}{j} \bar{\boldsymbol{\sigma}} \Delta j = \bar{\boldsymbol{\sigma}} \bar{\boldsymbol{F}}^T \boldsymbol{N}_{,x} \Delta \boldsymbol{q}. \tag{37}$$

4.3.2 Computation of $\bar{\boldsymbol{\Delta}}^{(2)}$.

First, we need to determine

$$\Delta \boldsymbol{S}^* = \frac{\partial \boldsymbol{S}^*}{\partial \boldsymbol{E}^*} \Delta \boldsymbol{E}^* = \boldsymbol{D}^* \Delta \boldsymbol{E}^*. \tag{38}$$

The components D^*_{mnkl} of the fourth-order tensor $\boldsymbol{D}$ of tangent moduli, together with the rotated second Piola-Kirchhoff stress tensor $\boldsymbol{S}^*$, are computed in the constitutive-equation software module as a function of the rotated Green-Lagrange strain $\boldsymbol{E}^*$. The tensor $\boldsymbol{D}^*$ verifies the following symmetries :

$$D^*_{mnkl} = D^*_{nmkl} = D^*_{mnlk}, \tag{39}$$

and can be mapped into a symmetric matrix in the following way :

$$
\bar{\boldsymbol{D}}^* =
\begin{bmatrix}
D^*_{1111} & D^*_{1122} & D^*_{1133} & D^*_{1112} & D^*_{1123} & D^*_{1131} \\
 & D^*_{2222} & D^*_{2233} & D^*_{2212} & D^*_{2223} & D^*_{2231} \\
 & & D^*_{3333} & D^*_{3312} & D^*_{3323} & D^*_{3331} \\
 & & & D^*_{1212} & D^*_{1223} & D^*_{1231} \\
 & \text{symmetric} & & & D^*_{2323} & D^*_{2331} \\
 & & & & & D^*_{3131}
\end{bmatrix}.
\tag{40}
$$

On the other hand, the variation of $\boldsymbol{E}^*$ is

$$
\Delta E^*_{ij} = \frac{1}{2}\Delta(F_{ik}F_{jk}) = \frac{1}{2}\left(\Delta F_{ik}F_{jk} + F_{ik}\Delta F_{jk}\right).
\tag{41}
$$

Using the differentiation rule for the inverse of a second order tensor, we obtain :

$$
\Delta F_{km} = -F_{kp}\Delta f_{pq}F_{qm}.
\tag{42}
$$

Introducing the latter equation into (41), it takes the form

$$
\begin{aligned}
\Delta E^*_{ij} &= -\frac{1}{2}\left(F_{il}\Delta f_{lm}F_{mk}F_{jk} + F_{ik}F_{jl}\Delta f_{lm}F_{mk}\right) \\
&= -I^F_{ijkl}\Delta f_{lm}F_{mk} = -I^F_{ijkl}\frac{\Delta f_{lm}F_{mk} + \Delta f_{km}F_{ml}}{2},
\end{aligned}
\tag{43}
$$

with

$$
I^F_{ijkl} = \frac{1}{2}\left(F_{il}F_{jk} + F_{ik}F_{jl}\right).
\tag{44}
$$

In matrix form, the variation of the rotated Green-Lagrange strain tensor then results :

$$
\begin{aligned}
\Delta\bar{\boldsymbol{E}}^* &=
\begin{bmatrix}
\Delta E^*_{11} \\
\Delta E^*_{22} \\
\Delta E^*_{33} \\
2\Delta E^*_{12} \\
2\Delta E^*_{23} \\
2\Delta E^*_{31}
\end{bmatrix} \\
&= -
\begin{bmatrix}
I^F_{1111} & I^F_{1122} & I^F_{1133} & I^F_{1112} & I^F_{1123} & I^F_{1131} \\
I^F_{2211} & I^F_{2222} & I^F_{2233} & I^F_{2212} & I^F_{2223} & I^F_{2231} \\
I^F_{3311} & I^F_{3322} & I^F_{3333} & I^F_{3312} & I^F_{3323} & I^F_{3331} \\
2I^F_{1211} & 2I^F_{1222} & 2I^F_{1233} & 2I^F_{1212} & 2I^F_{1223} & 2I^F_{1231} \\
2I^F_{2311} & 2I^F_{2322} & 2I^F_{2333} & 2I^F_{2312} & 2I^F_{2323} & 2I^F_{2331} \\
2I^F_{3111} & 2I^F_{3122} & 2I^F_{3133} & 2I^F_{3112} & 2I^F_{3123} & 2I^F_{3131}
\end{bmatrix}
\begin{bmatrix}
F_{m1}\Delta f_{1m} \\
F_{m2}\Delta f_{2m} \\
F_{m3}\Delta f_{3m} \\
F_{m1}\Delta f_{2m} + F_{m2}\Delta f_{1m} \\
F_{m2}\Delta f_{3m} + F_{m3}\Delta f_{2m} \\
F_{m3}\Delta f_{1m} + F_{m1}\Delta f_{3m}
\end{bmatrix} \\
&= -\bar{\boldsymbol{I}}^F\Delta\boldsymbol{a},
\end{aligned}
\tag{45}
$$

with

$$
\Delta\boldsymbol{a} =
\begin{bmatrix}
F_{11} & 0 & 0 & F_{21} & 0 & 0 & F_{31} & 0 & 0 \\
0 & F_{12} & 0 & 0 & F_{22} & 0 & 0 & F_{32} & 0 \\
0 & 0 & F_{13} & 0 & 0 & F_{23} & 0 & 0 & F_{33} \\
F_{12} & F_{11} & 0 & F_{22} & F_{21} & 0 & F_{32} & F_{31} & 0 \\
0 & F_{13} & F_{12} & 0 & F_{23} & F_{22} & 0 & F_{32} & F_{32} \\
F_{13} & 0 & F_{11} & F_{23} & 0 & F_{21} & F_{33} & 0 & F_{31}
\end{bmatrix}
\begin{bmatrix}
\Delta f_{11} \\
\Delta f_{21} \\
\Delta f_{31} \\
\Delta f_{12} \\
\Delta f_{22} \\
\Delta f_{32} \\
\Delta f_{13} \\
\Delta f_{23} \\
\Delta f_{33}
\end{bmatrix}
= \boldsymbol{F}^*\Delta\bar{\boldsymbol{f}} = \boldsymbol{F}^*\boldsymbol{N}_{,x}\Delta\boldsymbol{q}.
\tag{46}
$$

Therefore, the variation of $\boldsymbol{E}^*$ takes the form

$$\Delta \bar{\boldsymbol{E}}^* = -\bar{\boldsymbol{I}}^F \boldsymbol{F}^* \boldsymbol{N}_{,x} \Delta \boldsymbol{q}. \tag{47}$$

and the second term in the r.h.s. of equation (29) can be expressed in the matrix form

$$\bar{\boldsymbol{\Delta}}^{(2)} = j \bar{\boldsymbol{I}}^V \Delta \bar{\boldsymbol{S}}^* = -j \bar{\boldsymbol{I}}^V \bar{\boldsymbol{D}}^* \bar{\boldsymbol{I}}^F \boldsymbol{F}^* \boldsymbol{N}_{,x} \Delta \boldsymbol{q}. \tag{48}$$

4.3.3 Computation of $\bar{\boldsymbol{\Delta}}^{(3)}$.

First, let us rewrite the third term of the r.h.s. of equation (29) as follows :

$$\Delta_{kl}^{(3)} = j \Delta I_{klmn}^V S_{mn}^* = j H_{klpq} \Delta V_{pq}, \tag{49}$$

where

$$H_{klpq} = \left(I_{kmpq} V_{ln} + I_{lmpq} V_{kn} \right) S_{mn}^*, \tag{50}$$

with the fourth-order identity tensor

$$I_{kmpq} = \frac{1}{2} \left(\delta_{kp} \delta_{mq} + \delta_{kq} \delta_{mp} \right) \tag{51}$$

and δ_{kp} denoting the Kronecker delta.

The algorithmic matrix form of this term is then :

$$\bar{\boldsymbol{\Delta}}^{(3)} = \begin{bmatrix} j \Delta I_{11mn}^V S_{mn}^* \\ j \Delta I_{22mn}^V S_{mn}^* \\ j \Delta I_{33mn}^V S_{mn}^* \\ j \Delta I_{12mn}^V S_{mn}^* \\ j \Delta I_{23mn}^V S_{mn}^* \\ j \Delta I_{31mn}^V S_{mn}^* \end{bmatrix} = j \begin{bmatrix} H_{1111} & H_{1122} & H_{1133} & H_{1112} & H_{1123} & H_{1131} \\ H_{2211} & H_{2222} & H_{2233} & H_{2212} & H_{2223} & H_{2231} \\ H_{3311} & H_{3322} & H_{3333} & H_{3312} & H_{3323} & H_{3331} \\ H_{1211} & H_{1222} & H_{1233} & H_{1212} & H_{1223} & H_{1231} \\ H_{2311} & H_{2322} & H_{2333} & H_{2312} & H_{2323} & H_{2331} \\ H_{3111} & H_{3122} & H_{3133} & H_{3112} & H_{3123} & H_{3131} \end{bmatrix} \begin{bmatrix} \Delta V_{11} \\ \Delta V_{22} \\ \Delta V_{33} \\ \Delta V_{12} \\ \Delta V_{23} \\ \Delta V_{31} \end{bmatrix}$$
$$= j \ \bar{\boldsymbol{H}} \Delta \bar{\boldsymbol{V}}. \tag{52}$$

Now, it is only missing to compute $\Delta \boldsymbol{V}$. To this end, we begin by computing $\Delta \boldsymbol{V}^2$:

$$\Delta(V_{ik} V_{kj}) = \Delta V_{ik} V_{kj} + V_{ik} \Delta V_{kj} = A_{ijkm} \Delta V_{km}, \tag{53}$$

where

$$A_{ijkm} = \frac{1}{2} \left(\delta_{ik} V_{jm} + \delta_{jk} V_{im} + \delta_{im} V_{jk} + \delta_{jm} V_{ik} \right) = A_{ijmk} = A_{jikm}. \tag{54}$$

In matrix form, equation (53) takes the form :

$$\Delta \bar{\boldsymbol{V}}^2 = \begin{bmatrix} \Delta V_{11}^2 \\ \Delta V_{22}^2 \\ \Delta V_{33}^2 \\ 2\Delta V_{12}^2 \\ 2\Delta V_{23}^2 \\ 2\Delta V_{31}^2 \end{bmatrix} = \begin{bmatrix} A_{1111} & A_{1122} & A_{1133} & 2A_{1112} & 2A_{1123} & 2A_{1131} \\ A_{2211} & A_{2222} & A_{2233} & 2A_{2212} & 2A_{2223} & 2A_{2231} \\ A_{3311} & A_{3322} & A_{3333} & 2A_{3312} & 2A_{3323} & 2A_{3331} \\ 2A_{1211} & 2A_{1222} & 2A_{1233} & 4A_{1212} & 4A_{1223} & 4A_{1231} \\ 2A_{2311} & 2A_{2322} & 2A_{2333} & 4A_{2312} & 4A_{2323} & 4A_{2331} \\ 2A_{3111} & 2A_{3122} & 2A_{3133} & 4A_{3112} & 4A_{3123} & 4A_{3131} \end{bmatrix} \begin{bmatrix} \Delta V_{11} \\ \Delta V_{22} \\ \Delta V_{33} \\ \Delta V_{12} \\ \Delta V_{23} \\ \Delta V_{31} \end{bmatrix}$$
$$= \bar{\boldsymbol{A}} \Delta \bar{\boldsymbol{V}}. \tag{55}$$

On the other hand, since $\boldsymbol{V}^2 = 2\boldsymbol{E}^* - \boldsymbol{1}$, its variation can also be computed as

$$\Delta\bar{\boldsymbol{V}}^2 = 2\Delta\bar{\boldsymbol{E}}^* = -2\bar{\boldsymbol{I}}^F\boldsymbol{F}^*\boldsymbol{N}_{,x}\Delta\boldsymbol{q}. \tag{56}$$

By making (55) and (56) equal, we obtain

$$\Delta\bar{\boldsymbol{V}} = \bar{\boldsymbol{A}}^{-1}\Delta\bar{\boldsymbol{V}}^2 = -2\bar{\boldsymbol{A}}^{-1}\bar{\boldsymbol{I}}^F\boldsymbol{F}^*\boldsymbol{N}_{,x}\Delta\boldsymbol{q}. \tag{57}$$

Finally, the third term of the r.h.s. of equation (29) takes the matrix form :

$$\bar{\boldsymbol{\Delta}}^{(3)} = -2j\bar{\boldsymbol{H}}\bar{\boldsymbol{A}}^{-1}\bar{\boldsymbol{I}}^F\boldsymbol{F}^*\boldsymbol{N}_{,x}\Delta\boldsymbol{q}. \tag{58}$$

4.3.4   Final form of $\partial\bar{\boldsymbol{\sigma}}/\partial\boldsymbol{q}$

The form given to the terms $\bar{\boldsymbol{\Delta}}^{(i)}$ of the variation of $\bar{\boldsymbol{\sigma}}$ allows the immediate determination of the derivative of $\bar{\boldsymbol{\sigma}}$ with respect to the nodal unknowns $\boldsymbol{q}$:

$$\frac{\partial\bar{\boldsymbol{\sigma}}}{\partial\boldsymbol{q}} = \bar{\boldsymbol{\sigma}}\bar{\boldsymbol{F}}^T\boldsymbol{N}_{,x} - j\bar{\boldsymbol{I}}^V\bar{\boldsymbol{D}}^*\bar{\boldsymbol{I}}^F\boldsymbol{F}^*\boldsymbol{N}_{,x} - 2j\bar{\boldsymbol{H}}\bar{\boldsymbol{A}}^{-1}\bar{\boldsymbol{I}}^F\boldsymbol{F}^*\boldsymbol{N}_{,x}. \tag{59}$$

Therefore, the tangent stiffness matrix results

$$\boldsymbol{K} = \int_{\mathcal{B}}\boldsymbol{B}^T\left(\bar{\boldsymbol{\sigma}}\bar{\boldsymbol{F}}^T - j\bar{\boldsymbol{I}}^V\bar{\boldsymbol{D}}^*\bar{\boldsymbol{I}}^F\boldsymbol{F}^* - 2j\bar{\boldsymbol{H}}\bar{\boldsymbol{A}}^{-1}\bar{\boldsymbol{I}}^F\boldsymbol{F}^*\right)\boldsymbol{N}_{,x}\,\mathrm{d}v. \tag{60}$$

Note that $\boldsymbol{K}$ is non-symmetric, as it was already the case in references (Govindjee and Mihalic, 1996, 1998).

We remark that although not detailed in this work, the formulation can be easily extended to account also for thermal loads.

5   APPLICATION

5.1   Validation test

Let us consider the simple problem of bending a beam under plane strain conditions. First, we solve the direct problem, i.e., given the undistorted configuration $\mathcal{B}_0$ as well as the kinematic boundary conditions and the applied forces, we determine the distorted configuration $\mathcal{B}$. The problem is schematized in Figure 2. The domain is discretized using trilinear hexahedral finite elements. Even if it is essentially a 2D problem, 3D elements are used for the sake of generality. In order to represent the plane strain state, a one-element-wide mesh is used, and the faces normal to the $\boldsymbol{k}$-axis are constrained to move in the their planes.

Table 1: Material data for the beam bending problem.

$E_1 = 500\,\mathrm{N/cm}^2$	$\nu_{12} = 0.3$	$G_{12} = 192.31\,\mathrm{N/cm}^2$
$E_2 = 1000\,\mathrm{N/cm}^2$	$\nu_{23} = 0.2$	$G_{23} = 312.50\,\mathrm{N/cm}^2$
$E_3 = 750\,\mathrm{N/cm}^2$	$\nu_{13} = 0.25$	$G_{13} = 288.46\,\mathrm{N/cm}^2$

The bar is made of horizontal laminates with fibers disposed in the $\boldsymbol{i}$-direction. The material has an orthotropic behavior, characterized by the Young moduli E_1, E_2, E_3, Poisson ratii
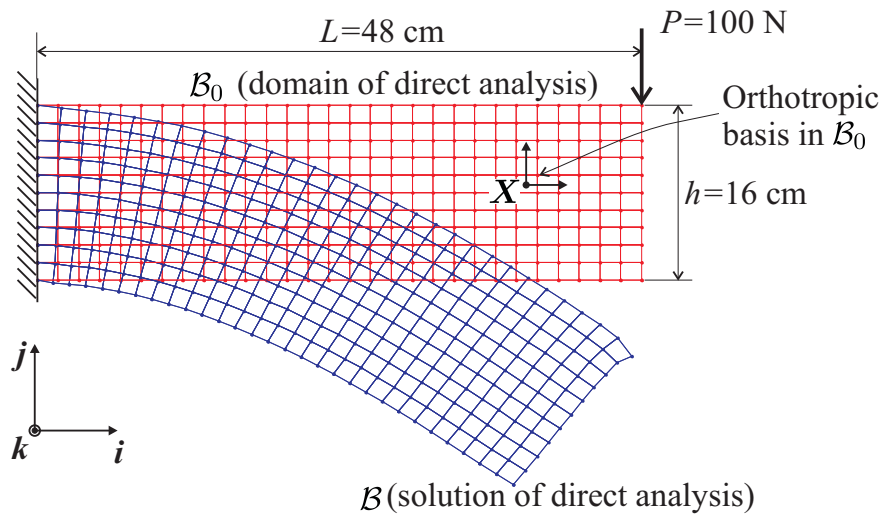
Figure 2: Direct problem.

μ_{12}, μ_{23}, μ_{13}, and shear ratii G_{12}, G_{23}, G_{13} with respect to the orthotropy orthogonal axes $\{\boldsymbol{u}^{(1)}, \boldsymbol{u}^{(2)}, \boldsymbol{u}^{(3)}\}$. Table 1 lists the values we assumed for these properties. Further, we adopt the hyperelastic constitutive law :

$$\bar{\boldsymbol{S}} = \bar{\boldsymbol{D}}\bar{\boldsymbol{E}}, \tag{61}$$

where

$$\bar{\boldsymbol{D}} = \begin{bmatrix} \frac{1-\nu_{23}\nu_{32}}{\alpha E_2 E_3} & \frac{\nu_{12}+\nu_{32}\nu_{13}}{\alpha E_1 E_3} & \frac{\nu_{13}+\nu_{12}\nu_{23}}{\alpha E_1 E_2} & 0 & 0 & 0 \\ & \frac{1-\nu_{13}\nu_{31}}{\alpha E_3 E_3} & \frac{\nu_{23}+\nu_{21}\nu_{13}}{\alpha E_1 E_2} & 0 & 0 & 0 \\ & & \frac{1-\nu_{12}\nu_{21}}{\alpha E_1 E_2} & 0 & 0 & 0 \\ & & & G_{12} & 0 & 0 \\ & \text{symmetric} & & & G_{23} & 0 \\ & & & & & G_{13} \end{bmatrix}, \tag{62}$$

with

$$\nu_{21} = \frac{E_2}{E_1}\nu_{12}, \qquad \nu_{31} = \frac{E_3}{E_1}\nu_{13}, \qquad \nu_{32} = \frac{E_3}{E_2}\nu_{23},$$

$$\alpha = \frac{1 - \nu_{12}\nu_{21} - \nu_{23}\nu_{32} - \nu_{13}\nu_{31} - 2\nu_{12}\nu_{32}\nu_{13}}{E_1 E_2 E_3}. \tag{63}$$

Here, the orthotropy axes $\{\boldsymbol{u}^{(1)}, \boldsymbol{u}^{(2)}, \boldsymbol{u}^{(3)}\}$ coincide with the Lagrangean principal axes, which are also coincident with the Cartesian coordinate basis $\{\boldsymbol{i}, \boldsymbol{j}, \boldsymbol{k}\}$.

The distorted configuration $\mathcal{B}$ computed as solution of the direct analysis and shown in Figure 2 becomes the domain of the inverse design analysis. The inverse problem is schematized in Figure 3. The objective of the computation is to verify if we are able to recover the original undistorted configuration as solution.

Regarding material properties, the orthotropy axes coincide now with the Eulerian principal axes $\boldsymbol{v}^{(i)} = \boldsymbol{R}\boldsymbol{u}^{(i)}$, where $\boldsymbol{R}$ is the rotational part of the deformation gradient $\boldsymbol{F}$ and varies throughout the domain. Although in this case the position of these axes can be exactly determined from the previous direct analysis, it could also be estimated from the distorted geometry taking into account the laminated nature of the body.
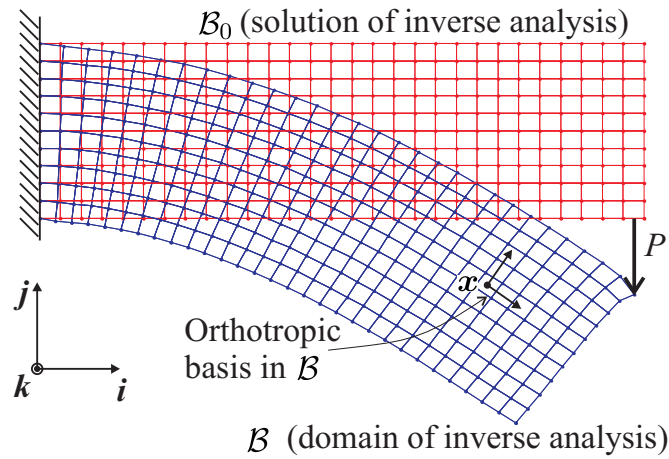
Figure 3: Inverse problem.
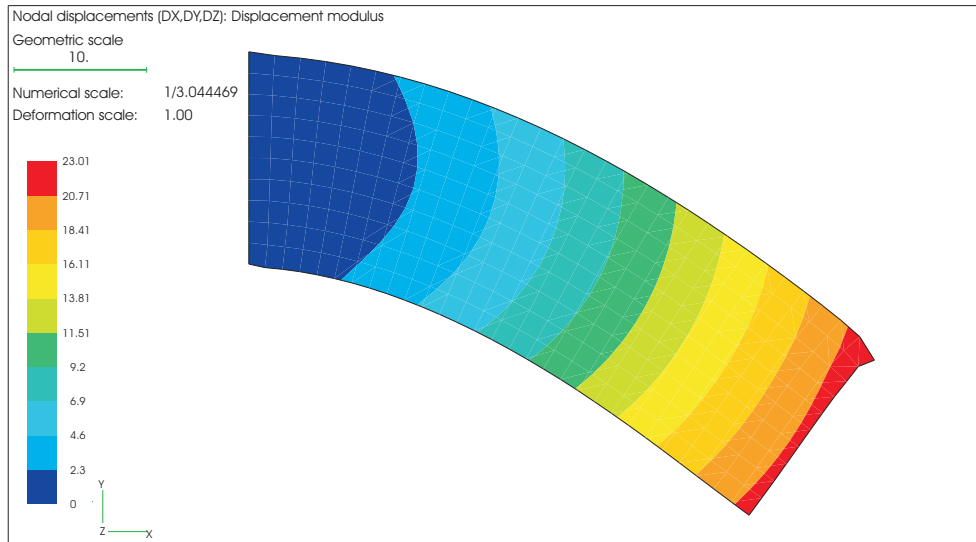
Figure 4: Displacement modulus from the inverse analysis.

The Eulerian counterpart of the constitutive equation (61) takes the form

$$\bar{\boldsymbol{S}}^* = \bar{\boldsymbol{D}}^* \bar{\boldsymbol{E}}^*, \tag{64}$$

where $\bar{\boldsymbol{D}}^*$ is the matrix of elastic moduli given in preferred directions coincident with the Eulerian or spatial axes, whose form is given by equation (62) and it is identical to $\bar{\boldsymbol{D}}$.

Figure 4 shows a plot of the inverse solution, displaying a map of the magnitude of the displacements $\boldsymbol{u} = \boldsymbol{x} - \boldsymbol{\psi}(\boldsymbol{x})$.

The error of the inverse model is defined as the distance between the nodes of the mesh used for the direct analysis and those of the undistorted mesh obtained as solution of the inverse analysis. After solving the equilibrium equation (12) with a very small residue norm $\|\boldsymbol{R}\| < 1.6 \times 10^{-11}$ (the L$_2$-norm of the residue vector $\boldsymbol{R}$), we obtained a maximum error of $26.6\,\mu$m at the nodes where the concentrated forces are applied. By comparing this value with the magnitude of the displacement at these nodes (23.01 cm), we note that the relative error is less than 0.01%, which demonstrates the excellent accuracy of the inverse model. Figure 5 shows the evolution of $\|\boldsymbol{R}\|$ along the iterative solution of the nonlinear equation (12). We note
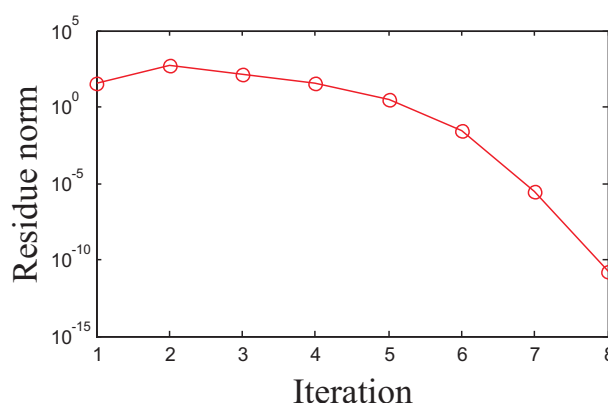
Figure 5: Evolution of the residue norm during the inverse analysis.

that after the 5th iteration, when the trial solution entered into the convergence radius of the solution, an optimal (quadratic) convergence rate is observed validating the computation of the tangent matrix $\boldsymbol{K}$.

5.2 Industrial application

The inverse model is applied now to a real case : the design of a laminated turbine blade, subjected to pressure and centrifugal forces. The blade has a complex shape determined by the fluid mechanics design for the loaded configuration. The objective of the computation is to determine the initial unloaded shape so that the blade shape in operation matches that imposed by the fluid mechanics design.

The material behavior is described using an hyperelastic constitutive law. The piece given in its desired distorted configuration is discretized using 40993 trilinear hexahedral finite elements, resulting a mesh of 52030 nodes. Figure 6 offers three views of the distorted blade geometry.

In Figure 7, the undistorted shape obtained from the inverse analysis is superposed to the distorted mesh. Let us note that geometrical and deformation scale are coincident in Figure 7, so that it gives an idea of the large magnitude of the deformations involved by the problem.

In order to solve the nonlinear equation (12), it was necessary to increase gradually the loading in four steps (the final step corresponding to the whole pressure and centrifugal loading applied to the blade), the solution of each step taken as initial guess for the following step. The inverse analysis has converged with an average of 3.5 iterations per step.

6 CONCLUSIONS

The present work introduces a finite element model for the inverse design analysis of three-dimensional geometrically nonlinear statics problems with hyperelastic materials.

Anisotropic materials can be treated without modifying the constitutive-equation software module developed for the classical (direct) large deformation elastic analysis.

The exact computation of the tangent matrix makes possible to obtain an optimum convergence rate.

An example showed the excellent accuracy of the model, measured by its ability to recover the original mesh of the corresponding direct analysis. Also, an example of application to the computation of the initial shape of a turbine blade subjected to pressure and centrifugal loads has been shown.
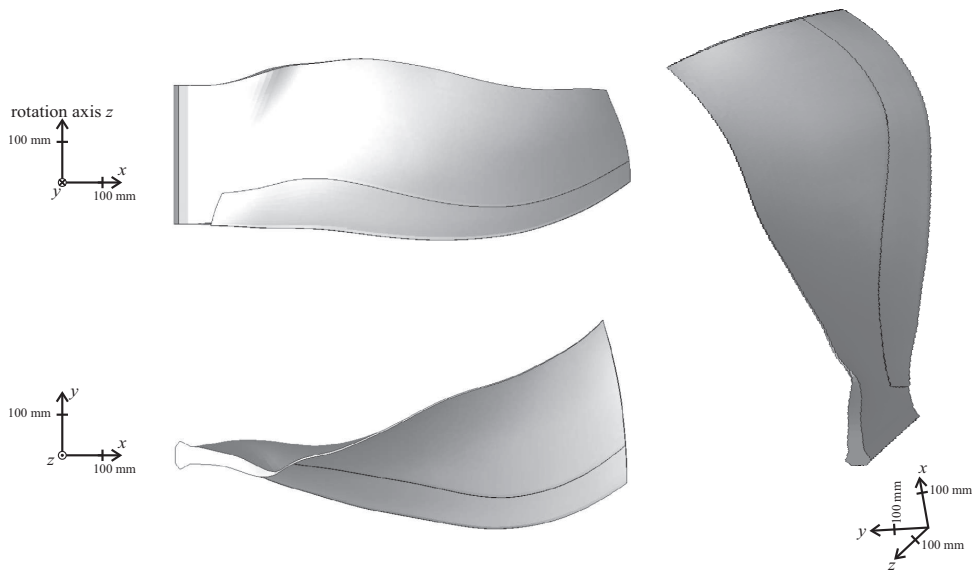
Figure 6: Inverse analysis of the turbine blade. Distorted shape from different points of view.
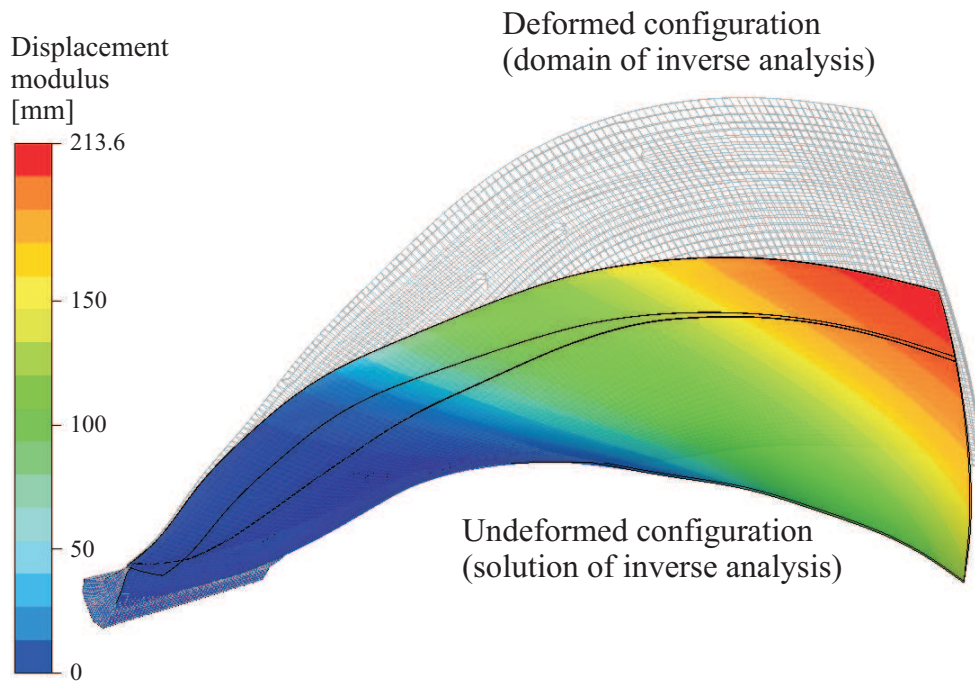
Figure 7: Inverse analysis of the turbine blade. Distorted vs. undistorted shapes and displacement modulus.

7   ACKNOWLEDGEMENTS

REFERENCES

J. V. Beck and K. A. Woodbury. Inverse problems and parameter estimation: integration of measurements and analysis. *Meas. Sci. Technol.*, 9:839–847, 1998.

S. Govindjee and P. A. Mihalic. Computational methods for inverse finite elastostatics. *Comput. Methods Appl. Mech. Engrg.*, 136:47–57, 1996.

S. Govindjee and P. A. Mihalic. Computational methods for inverse deformations in quasi-incompressible finite elasticity. *Int. J. Numer. Meth. Engng.*, 43:821–838, 1998.

R. W. Ogden. *Non-Linear Elastic Deformations*. Dover Publications, Inc., 1997.

Samtech. *Samcef / Mecano v11 User Manual*, 2005.

T. Yamada. Finite element procedure of initial shape determination for hyperelasticity. *Structural Engineering and Mechanics*, 6(2):173–183, 1997.

O. C. Zienkiewicz and R. L. Taylor. *The Finite Element Method*, volume 2: Solid and Structural Mechanics. Butterworth-Heinemann, 5th edition, 2000.